Raman vibrational spectra of bulk to monolayer ReS_2 with lower symmetry

Yanqing Feng,[1] Wei Zhou,[1] Yaojia Wang,[1] Jian Zhou,[2] Erfu Liu,[1] Yajun Fu,[1] Zhenhua Ni,[3] Xinglong Wu,[1] Hongtao Yuan,[4,5] Feng Miao,[1,*] Baigeng Wang,[1,*] Xiangang Wan,[1,*] and Dingyu Xing[1]

[1]*National Laboratory of Solid State Microstructures, School of Physics, Collaborative Innovation Center of Advanced Microstructures, Nanjing University, Nanjing 210093, China*

[2]*Department of Materials Science and Engineering, Nanjing University, Nanjing 210093, China*

[3]*Department of Physics, Southeast University, Nanjing 211189, China*

[4]*Geballe Laboratory for Advanced Materials, Stanford University, Stanford, California 94305, USA*

[5]*Stanford Institute for Materials and Energy Sciences, SLAC National Accelerator Laboratory, Menlo Park, California 94025, USA*

(Received 23 December 2014; revised manuscript received 11 May 2015; published 26 August 2015)

The lattice structure and symmetry of two-dimensional (2D) layered materials are of key importance to their fundamental mechanical, thermal, electronic, and optical properties. Raman spectroscopy, as a convenient and nondestructive tool, however, has its limitations in identifying all symmetry allowing Raman modes and determining the corresponding crystal structure of 2D layered materials with high symmetry, such as graphene and MoS_2. Due to the lower structural symmetry and extraordinary weak interlayer coupling of ReS_2, we successfully identify all 18 first-order Raman active modes for bulk and monolayer ReS_2. Without a van der Waals correction, our local density approximation (LDA) calculations successfully reproduce all the Raman modes. Our calculations also suggest no surface reconstruction effect and the absence of low frequency rigid-layer Raman modes below 100 cm^{-1}. Combining Raman spectroscopy and LDA thus provides a general approach for studying the vibrational and structural properties of 2D layered materials with lower symmetry.

DOI: 10.1103/PhysRevB.92.054110 PACS number(s): 61.50.Ah, 63.20.dd, 63.22.Np

I. INTRODUCTION

Two-dimensional (2D) layered materials have attracted a large amount of research interest due to their rich physics and tremendous application potentials [1–3]. As a nondestructive and powerful technique for characterizing the Brillouin-zone center (Γ-point) phonon properties of materials, Raman spectroscopy yields information about the structure, lattice symmetry, crystal quality, and the existence of defects and impurities [4–7]. It has also been widely used to understand the electronic and vibrational properties, as well as their dependence on the thickness of various 2D layered materials [8–12]. While lattice symmetry plays a crucial role in determining their fundamental properties, most experimentally investigated 2D layered materials have a high lattice symmetry, such as graphene and MoS_2. For these materials, usually there are low frequency rigid-layer Raman active modes below 100 cm^{-1} in the few-layer and bulk samples due to the stacking structure. These modes have very weak intensities, which presents a huge challenge for traditional Raman spectroscopy to experimentally identify all the symmetry allowing Raman active peaks given the strong Rayleigh scattering and special probing approaches needed [12–16]. For example, the crystalline structure of bulk MoS_2 belongs to the D_{6h}^4 space group and has two S-Mo-S single layers with four Raman active modes, namely, E_{1g}, A_{1g}, E_{2g}^1, and E_{2g}^2 modes [13,14]. Among these modes, the double-degenerate shear mode (E_{2g}^2 mode at 32 cm^{-1}) is almost negligible due to strong Rayleigh scattering [12]. In contrast, the 2D layered material ReS_2 was recently found [17] to have very weak interlayer coupling and a quite low symmetry. Using x-ray diffraction, Wildervanck and Jellinek [18] propose that bulk ReS_2 crystallizes in a triclinic structure with the space group $P\bar{1}$-C_i^1 (No. 2). This structure, with one unit cell containing one sandwich, had been confirmed by several groups [19–22]. With only one single layer in its unit cell, ReS_2 may exhibit novel and intriguing vibrational properties in Raman spectra.

In this paper, we systematically study the Raman spectra of bulk to monolayer ReS_2 samples. Due to the one single-layer structure in bulk ReS_2, ReS_2 shows no low frequency (below 100 cm^{-1}) rigid-layer vibrational Raman modes, in sharp contrast to other well-known members of the family of transition metal dichalcogenides (TMDs with the chemical formula MX_2, where M is a transition metal element and X is a chalcogenide element). Combining with local density approximation (LDA) calculations, we successfully identify all 18 symmetry allowing first-order Raman active peaks for bulk and monolayer ReS_2 in experiment. From monolayer to bulk, we observe that only two Raman modes exhibit measurably ($\sim$1.0 cm^{-1}) thickness induced frequency shifts, while many other modes have only tiny (0.5 or 0.6 cm^{-1}) shifts. Such results suggest a very weak interlayer interaction and no surface reconstruction in this layered material. The excellent agreement between the theoretical and experimental Raman results points to such an approach as a powerful tool to characterize the vibrational and structural properties of 2D layered materials with low symmetry.

II. METHODS

Raman experiments were performed using a 100× objective in a Horiba-JY T64000 system at ambient conditions. The excitation laser wavelength was 633 nm, with the laser power kept as 1 mW and a laser spot about 2 μm in diameter. The backscattering geometry was adopted in Raman measurements, with a spectrum resolution of 0.6 cm^{-1}. We

*Correspondence and requests for materials should be addressed to miao@nju.edu.cn; bgwang@nju.edu.cn; xgwan@nju.edu.cn

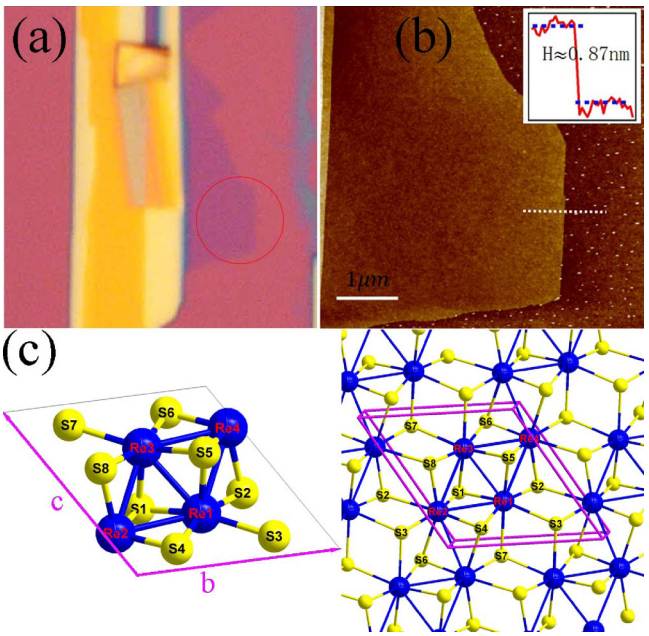

FIG. 1. (Color online) (a) A typical microscopic image of monolayer (in the red circle) and multilayer ReS_2 flakes on a Si substrate with 300 nm thick SiO_2. (b) An AFM image of the monolayer ReS_2 flake in the red circle of (a). Inset: The height probe profile of monolayer ReS_2, showing a monolayer ReS_2 height of 0.742 nm. (c) The lattice structure of bulk ReS_2. Left: Perspective drawing of a primitive cell of bulk ReS_2 down the interlayer lattice vector a. The vectors b and c are in-plane lattice vectors. Right: Periodical lattice structure of bulk ReS_2. The parallelepiped is the primitive cell of bulk ReS_2.

took the room temperature spectrum of every sample for 120 s, and analyzed the Raman peaks of the spectrum by the typical Lorentzian fitting procedure to get the corresponding Raman shift values.

Here, n-type single crystal ReS_2 were obtained using the Br_2 assisted chemical vapor transport method (see Ref. [17] for more details). We adopted the typical micromechanical exfoliation method to get few-layer ReS_2 flakes from the bulk ReS_2 crystal (2D semiconductors) on a Si substrate with 300 nm SiO_2 by the visual color differences between the samples and substrates. Using a Zeiss microscope (Scope A1), we could identify the ReS_2 flakes, and then determine their thickness by atomic force microscopy (AFM) (Bruker, multimode 8). In Fig. 1(a), an optical image of a typical single-layer ReS_2 flake is shown. Its thickness was determined to be 0.87 nm by AFM in the "ScanAsyst" mode [inset of Fig. 1(b)]. Since the interlayer distance of ReS_2 is 0.62 nm, we can thus confirm it is a monolayer flake.

Γ-point phonon frequencies calculations for few-layer (labeled as NL, where N is the layer number = 1,2,3,4 here) including bulk ReS_2 were performed by the small displacement method [23]. Instead of calculating the Raman tensor, based on the group theory, we analyzed the numerical phonon eigenvectors and obtained the Raman active modes. The calculations were performed in the framework of density functional theory (DFT), using the projector augmented wave (PAW) [24] method as implemented in the Vienna *ab initio* simulation package (VASP) code [25,26]. The basis set cutoff for the wave functions was 550 eV. Different exchange-correlation functions, such as the LDA scheme of Perdew and Zunger (CAPZ) [27], the generalized gradient approximation (GGA) schemes of Perdew-Burke (PB), Perdew-Burke-Ernzerhof (PBE) [28], and Perdew-Wang 91 (PW91) [29], were tested. Our numerical results show that among the above-mentioned GGA schemes, GGA-PW91 gives the best agreement with the experimental Raman results. Thus we only present the results of LDA and GGA-PW91. To check the influence of the van der Waals (vdW) interaction, we also include the vdW-corrected functions (vdW-DFT) and the Grimme corrections [30] to PBE in the theoretical calculations, and list the results in Table III for comparison. The few-layer ReS_2 were simulated with a vacuum of 15 Å in the interlayer x direction to ensure a negligible interaction between their periodic images. The Brillouin-zone integration was done on uniform Monkhorst-Pack grids of $1\times24\times24$ for few-layer ReS_2 and $24\times24\times24$ for bulk ReS_2. The convergence criterion of self-consistent calculations for ionic relaxations was 10^{-5} eV between two consecutive steps. The internal coordinates and lattice constants were fully relaxed for bulk ReS_2. For few-layer ReS_2, we relaxed the internal coordinates and lattice constants with the fixing volume method to avoid the collapse of the vacuum. The convergence criterion of relaxation was that the pressures on the lattice unit cell were less than 0.5 kbar and the Hellman-Feynman forces on the ions were less than 0.001 eV/Å.

III. RESULTS AND DISCUSSION

As shown in Fig. 1(c), this structure can be thought as distorted 1T-MX_2 dichalcogenides, and the only symmetry operation for this material is the inversion with the center located in the middle of a Re1-Re3 bond. We started by optimizing the lattice structure. The numerical lattice parameters and independent internal atomic coordinates for bulk ReS_2, as well as the experimentally obtained results [20], are listed in Table I. We find that the standard LDA method successfully reproduces the internal coordinates and lattice constants, while the GGA scheme significantly overestimates a by about 15.1% and the vdW-DFT method gives a smaller value than the LDA and the experimental ones. Each Re of ReS_2 has six neighboring S sites, but, different from the case in MoS_2, the Re-S bond lengths are not equal to each other. The Re1 site bonds with S1, S2, S3, S4, S5, and S7, and the LDA bond lengths are 2.33, 2.36, 2.44, 2.40, 2.34, and 2.42 Å, respectively; Re2-Si (i = 1,2,3,4,6,8) bond distances are 2.34, 2.46, 2.40, 2.38, 2.31, and 2.51 Å, respectively. However, the average lengths are approximately the same for the two independent Re-S bonds (2.38 Å for Re1-S and 2.39 Å for Re2-S), which are shorter than the Mo-S bond in MoS_2 (2.42 Å [14]). Meanwhile, each Re atom has three neighboring Re sites and there are four Re atoms in the unit cell. They participate in bonding and form a parallelogram-shaped Re4 cluster, leading to a single-layer structure per unit cell as shown in Fig. 1(c) [17]. The Re-Re bonding lengths are listed in Table II (similarly, the LDA and vdW-DFT underestimate the Re-Re bonds while the GGA slightly overestimates the Re-Re bonds). This forming of a Re4 cluster brings a significant amount of

TABLE I. The relaxed lattice parameters and independent fractional coordinates of bulk ReS_2 with DFT-LDA, vdW-DFT, and DFT-GGA methods. The experimental data [20] are listed for comparison. The lengths are in units of Å.

Lattice parameter		a	b	c	α	β	γ
LDA		6.315	6.482	6.415	121.4°	88.3°	106.6°
vdW-DFT		6.308	6.482	6.414	121.4°	88.3°	106.6°
GGA		7.389	6.588	6.527	121.3°	88.1°	105.0°
Expt. [20]		6.417	6.510	6.461	121.1°	88.4°	106.5°
Fractional coordinates	Bulk	Re1	Re2	S1	S2	S3	S4
X	LDA	0.503	0.492	0.210	0.276	0.696	0.761
	vdW-DFT	0.503	0.492	0.209	0.276	0.697	0.761
	GGA	0.502	0.492	0.252	0.309	0.667	0.722
	Expt. [20]	0.503	0.493	0.217	0.277	0.698	0.756
Y	LDA	0.513	0.058	0.250	0.774	0.754	0.279
	vdW-DFT	0.513	0.058	0.250	0.774	0.755	0.279
	GGA	0.512	0.058	0.262	0.783	0.746	0.266
	Expt. [20]	0.511	0.056	0.250	0.771	0.753	0.273
Z	LDA	0.298	0.247	0.366	0.383	0.119	0.119
	vdW-DFT	0.298	0.247	0.366	0.383	0.119	0.119
	GGA	0.298	0.247	0.374	0.390	0.114	0.115
	Expt. [20]	0.297	0.248	0.368	0.384	0.117	0.118

bond charges between the Re-Re dimers [17]. From Fig. 1(c) we also see that different S atoms have completely different environments and span different Re-Re bond numbers: S1 spans three metal-metal bonded Re atoms (Re1-Re2, Re1-Re3, and Re2-Re3); S2 and S4 span a single metal-metal bond (Re1-Re4 for S2, Re1-Re2 for S4); and S3 is a little isolated and spans no metal-metal bonds. All these structure properties for bulk ReS_2 are quite different from MX_2 dichalcogenides such as $1T$-MX_2 [31], $2H$-MX_2 [12,32], and $3R$-MX_2 [33,34].

The nonresonant Raman scattering measurement results on bulk ReS_2 are shown in Fig. 2(a). Due to the limitation of the spectrometer, we can only measure the Raman modes above 100 cm^{-1}, shown in Fig. 2(a). The strongest peak located at 520.7 cm^{-1} comes from the silicon substrate. Similar to the results of Tongay *et al.* [17], we also found that there are two big Raman peaks located around 150 and 200 cm^{-1}. By carefully collecting the signals, we eventually observed 18 modes spreading in the 100−450 cm^{-1} range. We mark these observable Raman active modes by arrows in Fig. 2(a), and list their frequencies in Table III.

There are 12 atoms in the unit cell, thus bulk ReS_2 possesses 36 vibrational modes. ReS_2 is isomorphic to the point group C_i (the Schoenflies character tables for the point groups can be found in Ref. [35]), and according to decomposition [36] and group theory symmetry analysis, the irreducible representations of the 36 Γ-point phonon modes can be written as $\Gamma = 18(A_g + A_u)$. There are 18 asymmetric A_u modes and 18 symmetric A_g modes with respect to inversion. Three acoustical modes and infrared active optical modes must be asymmetric under inversion. Thus 15 infrared active and 18 Raman modes can be found in bulk ReS_2. It is worth noting that for ReS_2 all of the Raman active and infrared active modes are nondegenerate, while for the common MX_2 dichalcogenides, such as $2H$-MoS_2, there exist two-degenerate E symmetry in-plane vibrational modes (E^1_{2g} and E^2_{2g}) [12,13] besides the nondegenerate A_g modes due to the highly symmetric lattice structure.

TABLE II. The relaxed independent Re-Re bond lengths (the lengths of Re2-Re3 and Re3-Re4 equate to Re1-Re4 and Re1-Re2, respectively, a result of inversion symmetry) given by DFT-LDA, vdW-DFT, and DFT-GGA methods. The experimental data [20] are listed for comparison. The lengths are in units of Å.

Re-Re distance	Re1-Re2	Re1-Re3	Re1-Re4
LDA	2.77	2.68	2.78
vdW-DFT	2.77	2.68	2.78
GGA	2.82	2.72	2.84
Expt. [20]	2.79	2.69	2.82

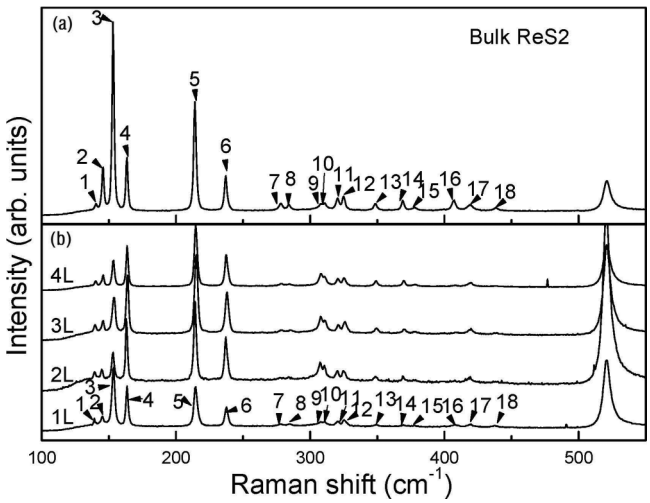

FIG. 2. (a) Raman spectrum of bulk ReS_2. The arrows mark the concrete positions of 18 Raman active modes of bulk ReS_2. (b) Raman spectra of few-layer ReS_2. The arrows mark the concrete positions of 18 Raman active modes of monolayer ReS_2.

TABLE III. The 18 Raman active frequencies (in units of cm^{-1}) in bulk ReS_2 of experimental measurements under a 633 nm solid state excitation wavelength laser and first-principles theoretical calculations. The A_g-like, E_g-like, and Cp modes are also marked correspondingly.

	Bulk Raman frequency				1L Raman frequency		
Symmetry	Expt.	LDA	vdW-DFT	GGA	Expt.	LDA	GGA
A_g-like	140.3	136.8	137.2	129.4	139.2	132.7	129.3
A_g-like	145.9	144.5	145.3	137.1	145.3	142.4	137.2
E_g-like	153.1	153.6	154.0	148.0	153.6	155.5	148.3
E_g-like	163.6	163.4	163.6	158.4	163.6	164.3	158.4
E_g-like	217.2	218.2	218.3	208.7	217.7	220.2	208.9
E_g-like	237.1	238.1	238.0	228.4	237.7	241.3	228.7
Cp	278.3	275.1	276.4	261.5	278.3	275.6	261.9
Cp	284.2	282.6	283.5	268.5	284.7	282.8	268.8
E_g-like	307.8	308.5	311.9	295.8	307.8	309.6	295.9
E_g-like	311.0	312.1	312.9	298.3	311.0	311.8	298.2
Cp	320.6	318.3	319.8	303.2	320.6	317.4	303.5
Cp	324.9	325.8	327.2	311.1	324.9	326.9	311.1
Cp	348.8	349.7	351.3	332.4	348.8	350.4	332.7
Cp	368.9	370.4	372.8	354.5	369.5	371.6	354.7
Cp	377.9	381.3	382.8	363.0	377.4	380.3	363.3
Cp	407.3	408.7	412.0	393.4	408.3	410.8	393.5
A_g-like	418.7	422.3	425.1	406.7	419.3	423.8	406.8
A_g-like	438.0	443.4	446.1	425.1	437.5	443.7	424.7

To further answer the questions as to whether there are first-order Raman modes located below 100 cm^{-1} and whether 18 observed Raman modes above 100 cm^{-1} are all first-order modes, we performed LDA, vdW-DFT, and GGA Γ-point phonon calculations based on our optimized structure. It is found that among all 36 modes, except the three acoustic modes, all the other modes are above 100 cm^{-1}, and we present the numerical frequencies of the 18 A_g modes in Table III. It is found that both the LDA and vdW-DFT methods calculated frequencies that perfectly agree with experimental results. The maximal discrepancy between the LDA and experimental data is only 5.4 cm^{-1} from the A_g mode around 443.4 cm^{-1}, and most of the differences are less than 2.0 cm^{-1}. Thus we believe that the standard LDA, without considering the vdW interaction, is already sufficient to describe the geometric structure and the mechanical properties for this weakly interlayer coupled layered material. Tan *et al.* [10] and Luo *et al.* [37] also confirmed that the LDA scheme can predict reasonable lattice constants and also reproduce good Raman frequencies that match with the experimental results. On the other hand, the GGA calculations considerably underestimate the Raman frequencies, as shown in Table III. Thus, from here on, we focus on the LDA results.

Since all the calculated Raman mode frequencies agree very well with the experimental data, we conclude that the 18 experimental peaks, marked in Fig. 2(a) and listed in Table III, are the 18 symmetry allowing first-order Raman modes. Also, although due to the limitations of our equipment we cannot measure the low frequency Raman mode, we can still conclude that there are no low frequency rigid-layer Raman modes [38] below 100 cm^{-1} due to the fact the unit cell of bulk ReS_2 has only one layer. We can further expect that for the MX_2 dichalcogenides with a distorted $1T$ structure, such as $ReSe_2$ [39] and TcS_2 [39], such Raman modes also should be absent. On the other hand, for those layered compounds whose unit cells have two layers, low frequency E_{2g} rigid-layer shear Raman vibrational modes exist. Some examples include the modes of about 42 cm^{-1} for graphite [10,38], about 52 cm^{-1} in bulk h-BN [40,41], about 32 cm^{-1} in bulk MoS_2 [12,14], and 22 cm^{-1} in bulk WSe_2 [12].

By checking the phonon eigenvectors, we now analyze the Raman modes. Although, according to the symmetry, all of the Raman active modes of ReS_2 belong to the A_g mode, we still denote the one with large out-of-plane vibrational weights as the A_g-like mode, with large in-plane vibrational weights as the E_g-like mode, and with both strong in-plane and out-of-plane vibrational weights as the Cp mode [17]. (Cp stands for simplicity of in-plane and out-of-plane coupled mode.) The Re atom is much heavier than the S atom, and there are clearly two panels in the phonon spectrum of ReS_2, as shown in Ref. [17]. The top 24 branches above 250 cm^{-1} are mainly contributed by S motions, while the 12 branches below 250 cm^{-1} basically come from Re vibrations. Our numerical results show that from low frequency to high frequency, the vibrational weights of S atoms increase and Re atoms decrease gradually. As shown in Table III, there are four A_g-like modes. Two low frequency A_g-like modes (136.8 and 144.5 cm^{-1}) mainly involve the out-of-plane vibrations of Re atoms, and the high frequency A_g-like modes (422.3 and 443.4 cm^{-1}) mainly involve the out-of-plane vibrations of S atoms. The E_g-like modes, located at 153.6, 163.4, 218.2, and 238.1 cm^{-1}, mainly involve in-plane vibrations of Re atoms, while the other two E_g-like modes, at 308.5 and 312.1 cm^{-1}, are mainly in-plane vibrations of S atoms. These frequency distributions of E_g-like modes are similar to the results reported by Tongay *et al.* [17], except for one E_g-like Raman mode at 218.2 cm^{-1} (213 cm^{-1} in the Raman spectrum of Tongay *et al.* [17], which was treated as an A_g-like mode with mostly out-of-plane vibrations). The Cp modes at 275.1 and 282.6 cm^{-1} involve in-plane and out-of-plane vibrations of Re and S atoms, while the Cp modes above 300 cm^{-1} are mainly in-plane and out-of-plane vibrations of S atoms.

We show several typical vibrational modes in Fig. 3. The E_g-like mode at 153.6 cm^{-1} mainly involves in-plane stretching vibrations of Re-Re bonds along the edge of the Re4 unit, and in-plane vibrations of a pair of S atoms (S1 and S5) atoms as well. The E_g-like modes at 163.4 and 218.2 cm^{-1} involve in-plane stretching vibrations of Re-Re bonds, and the vibrations of the pair of S atoms which span only one metal-metal bond. The E_g-like mode at 238.1 cm^{-1} vibrates mainly along the diagonal line of the Re4 unit with little S atom vibrations. Different S atom vibrations span different numbers of the Re-Re dimers, leading to different amounts of bond charge polarizations and thus different Raman intensities. Hence, the E_g-like modes at 153.6, 163.4, and 218.2 cm^{-1} are strong Raman peaks in the Raman spectrum shown in Fig. 2(a). The 153.6 cm^{-1} peak has the strongest intensity. The A_g-like mode at 144.5 cm^{-1} also displays a relatively strong intensity, as shown in Fig. 2(a), due to the participation of the pair of S1 and S5 atom in-plane stretching vibrations, while the A_g-like mode at 136.8 cm^{-1} does not involve S atom vibrations and thus shows a weak signal.

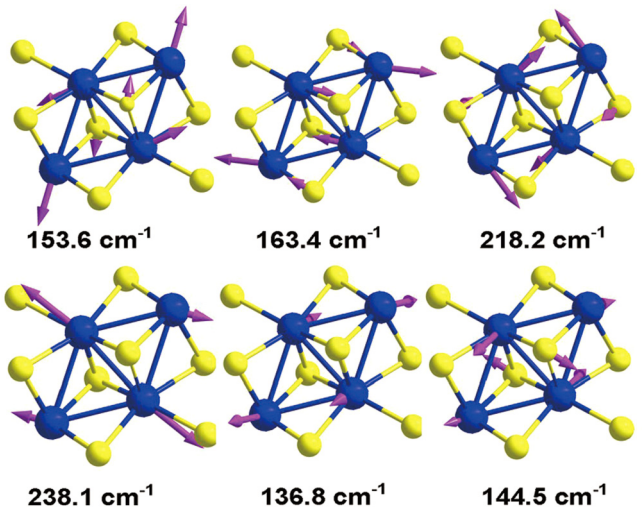

FIG. 3. (Color online) Four E_g-like vibrational modes at 153.6, 163.4, 218.2, and 238.1 cm^{-1} and two A_g-like vibrational modes at 136.8 and 144.5 cm^{-1} for bulk ReS_2, from LDA theoretical calculations and analysis of the vibrational eigenvectors. The lengths of the arrows are proportional to the modular of the phonon eigenvectors, with length weights less than 15% ignored.

We also studied the Raman spectra of few-layer and monolayer ReS_2 systems, which have inversion symmetry regardless of whether the layer number is even or odd, unlike MoS_2 [12]. We performed a structural optimization and list the numerical results for monolayer ReS_2 in Table IV. To the best of our knowledge, there is no experimental measurement on the lattice parameters for monolayer ReS_2, so we listed previous theoretical data for comparison [17,42]. Our numerical results agree well with the previous theoretical results. As shown in Tables I and IV, the differences between the numerical results of bulk and monolayer ReS_2 are quite small.

The Raman spectrum of monolayer ReS_2 is shown in Fig. 2(b) and the observable 18 Raman active peaks are marked with arrows. We list the concrete frequencies in Table III. The monolayer ReS_2 shows a very similar Raman spectrum to that of the bulk one in the 100−450 cm^{-1} range without new peaks, indicating that the symmetry remains consistent when going from bulk to monolayer. Our experimental results show that the first A_g-like mode exhibits an obvious redshift as the thickness decreases from the bulk to monolayer and softens by 1.1 cm^{-1}. The 16th Cp mode exhibits about a 1.0 cm^{-1} blueshift. Many other modes have tiny (0.5 or 0.6 cm^{-1}) thickness induced frequency shifts. Our theoretical calculations shown in Table III give the same frequency shifts. These results indicate the absence of surface reconstruction. In contrast, in MoS_2 systems, the surface reconstruction [43] softens the A_g mode of the topmost layer by 25 cm^{-1} [8].

TABLE IV. The relaxed lattice parameters of monolayer ReS_2 with DFT-LDA and DFT-GGA methods. The VASP GGA-PBE results by Tongay *et al.* [17] and Horzum *et al.* [42] are listed for comparison. The lengths are in units of Å.

Lattice parameter	a	b	c	α	β	γ
LDA		6.477	6.408	121.4°	88.1°	106.2°
GGA		6.587	6.526	121.3°	88.1°	107.0°
GGA [17]		6.51	6.41			
GGA [42]		6.51	6.40			

We next conducted a systematic Raman spectra study of few-layer (from 2L to 4L) ReS_2 flakes, which are also shown in Fig. 2(b). It shows similar Raman spectra to that of bulk and monolayer ReS_2, with 18 corresponding observable Raman active modes in the 100−450 cm^{-1} range. As the layer number N increases, there are $12N$ atoms and $36N$ vibrational modes in NL, with the point group C_i,$\Gamma = 18N(A_g + A_u)$, and there should be $18N$ nondegenerate first-order Raman A_g modes. But the differences in the increased Raman modes between the NL ($N \geqslant 2$) and monolayer are tiny beyond the spectrum resolution, together with the tiny thickness induced frequency shifts and structural optimization and Raman frequency differences discussed above, suggesting an ultraweak interlayer interaction. Our experimental and numerical results are consistent with recent work [17,44], where the monolayer behavior and ultraweak interlayer interaction in bulk ReS_2 due to electronic and vibrational decoupling were explored. Meanwhile, from bulk to monolayer, we do not notice any regular and distinct thickness dependent tendency of the linewidths and the peak intensities of all 18 Raman active peaks.

It is worth mentioning that there is also work reporting a different crystal structure [45]. Very recently, low frequency interlayer modes had been reported in $ReSe_2$ [46], but it had been suggested that ReS_2 is not isostructural with $ReSe_2$ (see Ref. [20]). Based on the structure with 24 atoms per unit cell [45], we thus also performed the calculations. The most distinct difference between the Raman spectra from one sandwich per unit cell [18–22] and two sandwiches per unit cell [45] is the presence of a low frequency interlayer mode (around 35.8 cm^{-1}), which is much below the spectrometer low limit of 100 cm^{-1} of our commercial Horiba-JY T64000 system. Thus, experimentally searching the low frequency Raman mode will finally and unambiguously identify the structure of ReS_2 in the future.

IV. CONCLUSION

In conclusion, we presented both DFT and experimental Raman scattering studies on lattice vibrations of bulk to monolayer ReS_2, which is a 2D TMD material with a low lattice symmetry. Combining with LDA calculations, we successfully identified all symmetry allowing Raman modes for both bulk and monolayer ReS_2. We find that the low frequency rigid-layer vibrational modes are nonexistent in this low symmetry bulk ReS_2 and, due to the rather weak interlayer interaction, the thickness induced frequency shifts are rather small and there is no surface reconstruction. We believe that combining Raman measurements and LDA calculations is an efficient way for studying the vibrational and structural properties of 2D layered materials with low symmetry.

ACKNOWLEDGMENT

The work is supported by the National Key Project for Basic Research of China (Grants No. 2011CB922101,

No. 2015CB921600, and No. 2013CBA01603), the National Natural Science Foundation of China (Grants No. 91122035, No. 11374142, No. 11174124, No. 11374137, and No. 11474150), the Natural Science Foundation of Jiangsu Province (BK20130544 and BK20140017), the Specialized Research Fund for the Doctoral Program of Higher Education (20130091120040), and Fundamental Research Funds for the Central Universities. H.T.Y. was supported by the Department of Energy, Office of Basic Energy Sciences, Division of Materials Sciences and Engineering, under Contract No. DE-AC02-76SF00515. The project is also funded by Priority Academic Program Development of Jiangsu Higher Education Institutions. We also acknowledge the support for the computational resources by the High Performance Computing Center of Nanjing University.

Y.F. and W.Z. contributed equally to this work.

[1] K. S. Novoselov, D. Jiang, F. Schedin, T. J. Booth, V. V. Khotkevich, S. V. Morozov, and A. K. Geim, Proc. Natl. Acad. Sci. USA **102**, 10451 (2005).
[2] A. H. Castro Neto, F. Guinea, N. M. R. Peres, K. S. Novoselov, and A. K. Geim, Rev. Mod. Phys. **81**, 109 (2009).
[3] M. Chhowalla, H. S. Shin, G. Eda, L. J. Li, K. P. Loh, and H. Zhang, Nat. Chem. **5**, 263 (2013).
[4] D. Wolverson, S. Crampin, A. S. Kazemi, A. Ilie, and S. J. Bending, ACS Nano **8**, 11154 (2014).
[5] T. Sander, S. Eisermann, B. K. Meyer, and P. J. Klar, Phys. Rev. B **85**, 165208 (2012).
[6] X. Luo, Y. Y. Zhao, J. Zhang, M. Toh, C. Kloc, Q. H. Xiong, and S. Y. Quek, Phys. Rev. B **88**, 195313 (2013).
[7] A. C. Ferrari, Solid State Commun. **143**, 47 (2007).
[8] C. Lee, H. Yan, L. E. Brus, T. F. Heinz, J. Hone, and S. Ryu, ACS Nano **4**, 2695 (2010).
[9] A. C. Ferrari, J. C. Meyer, V. Scardaci, C. Casiraghi, M. Lazzeri, F. Mauri, S. Piscanec, D. Jiang, K. S. Novoselov, S. Roth, and A. K. Geim, Phys. Rev. Lett. **97**, 187401 (2006).
[10] P. H. Tan, W. P. Han, W. J. Zhao, Z. H. Wu, K. Chang, H. Wang, Y. F. Wang, N. Bonini, N. Marzari, N. Pugno, G. Savini, A. Lombardo, and A. C. Ferrari, Nat. Mater. **11**, 294 (2012).
[11] C. H. Lui, M. M. Leandro, S. H. Kim, G. Lantz, F. E. Laverge, R. Saito, and T. F. Heinz, Nano Lett. **12**, 5539 (2012).
[12] Y. Y. Zhao, X. Luo, H. Li, J. Zhang, P. T. Araujo, C. K. Gan, J. Wu, H. Zhang, S. Y. Quek, M. S. Dresselhaus, and Q. H. Xiong, Nano Lett. **13**, 1007 (2013).
[13] J. L.Verble and T. J. Wieting, Phys. Rev. Lett. **25**, 362 (1970).
[14] H. L. Zeng, B. Zhu, K. Liu, J. H. Fan, X. D. Cui, and Q. M. Zhang, Phys. Rev. B **86**, 241301(R) (2012).
[15] G. Plechinger, S. Heydrich, J. Eroms, D. Weiss, C. Schüller, and T. Korn, Appl. Phys. Lett. **101**, 101906 (2012).
[16] X. Zhang, W. P. Han, J. B. Wu, S. Milana, Y. Lu, Q. Q. Li, A. C. Ferrari, and P. H. Tan, Phys. Rev. B **87**, 115413 (2013).
[17] S. Tongay, H. Sahin, C. Ko, A. Luce, W. Fan, K. Liu, J. Zhou, Y.-S. Huang, C.-H. Ho, J. Y. Yan, D. F. Ogletree, S. Aloni, J. Ji, S. S. Li, J. B. Li, F. M. Peeters, and J. Q. Wu, Nat. Commun. **5**, 4252 (2014).
[18] J. C. Wildervanck and F. Jellinek, J. Less-Common Met. **24**, 73 (1971).
[19] S. P. Kelty, A. F. Ruppert, R. R. Cbianelli, J. Ren, and M.-H. Whangbo, J. Am. Chem. Soc. **116**, 7857 (1994).
[20] H. H. Murray, S. P. Kelty, and R. R. Cbianelli, Inorg. Chem. **33**, 4418 (1994).
[21] C. H. Ho, Y. S. Huang, P. C. Liao, and K. K. Tiong, J. Phys. Chem. Solids **60**, 1797 (1999).
[22] D. B. Hou, Y. Z. Ma, J. G. Du, J. Y. Yan, C. Ji, and H. Y. Zhu, J. Phys. Chem. Solids **71**, 1571 (2010).
[23] G. Kresse, J. Furthmuller, and J. Hafner, Europhys. Lett. **32**, 729 (1995).
[24] G. Kresse and D. Joubert, Phys. Rev. B **59**, 1758 (1999).
[25] G. Kresse and J. Hafner, Phys. Rev. B **47**, 558 (1993).
[26] G. Kresse and J. Furthmuller, Phys. Rev. B **54**, 11169 (1996).
[27] J. P. Perdew and A. Zunger, Phys. Rev. B **23**, 5048 (1981).
[28] J. P. Perdew, K. Burke, and M. Ernzerhof, Phys. Rev. Lett. **77**, 3865 (1996).
[29] J. P. Perdew and Y. Wang, Phys. Rev. B **45**, 13244 (1992).
[30] S. J. Grimme, Comput. Chem. **27**, 1787 (2006).
[31] J. A. Wilson, Phys. Status Solidi B **86**, 11 (1978).
[32] J. L. Verble, T. J. Wieting, and J. T. Reed, Solid State Commun. **11**, 941 (1972).
[33] J.-J. He, K. Hummer, and C. Franchini, Phys. Rev. B **89**, 075409 (2014).
[34] S. K. Srivastava and B. N. Avasthi, J. Mater. Sci. Lett. **20**, 3801 (1985).
[35] M. S. Dresselhaus, G. Dresselhaus, and A. Jorio, *Group Theory: Application to the Physics of Condensed Matter* (Springer, Berlin, 1986).
[36] S. H. Chen, Phys. Rev. **163**, 532 (1967).
[37] X. Luo, Y. Y. Zhao, J. Zhang, Q. H. Xiong, and S. Y. Quek, Phys. Rev. B **88**, 075320 (2013).
[38] K. H. Michel and B. Verberck, Phys. Rev. B **85**, 094303 (2012).
[39] C. M. Fang, G. A. Wiegers, C. Haas, and R. A. de Groot, J. Phys.: Condens. Matter **9**, 4411 (1997).
[40] J. Serrano, A. Bosak, R. Arenal, M. Krisch, K. Watanabe, T. Taniguchi, H. Kanda, A. Rubio, and L. Wirtz, Phys. Rev. Lett. **98**, 095503 (2007).
[41] R. Geick, C. H. Perry, and G. Rupprecht, Phys. Rev. **146**, 543 (1966).
[42] S. Horzum, D. Cakir, J. Suh, S. Tongay, Y.-S. Huang, C.-H. Ho, J. Wu, H. Sahin, and F. M. Peeters, Phys. Rev. B **89**, 155433 (2014).
[43] B. J. Mrstik, R. Kaplan, T. L. Reinecke, M. Van Hove, and S. Y. Tong, Phys. Rev. B **15**, 897 (1977).
[44] E. F. Liu, Y. J. Fu, Y. J. Wang, Y. Q. Feng, H. M. Liu, X. G. Wan, W. Zhou, B. G. Wang, L. B. Shao, C.-H. Ho, Y.-S. Huang, Z. Y. Gao, L. G. Wang, A. D. Li, J. W. Zeng, F. Q. Song, X. R. Wang, Y. Shi, H. T. Yuan, Y. H. Harold, Y. Cui, F. Miao, and D. Y. Xing, Nat. Commun. **6**, 6991 (2015).
[45] H. J. Lamfers, A. Meetsma, G. A. Wiegers, and J. L. de Boer, J. Alloys Compd. **241**, 34 (1996).
[46] H. Zhao, J. B. Wu, H. X. Zhong, Q. S. Guo, X. M. Wang, F. N. Xia, L. Yang, P.-H. Tan, and H. Wang, arXiv:1504.07664.